# Modelling and optimal control system design for quadrotor platform – an extended approach

## R. ZAWISKI* and M. BŁACHUTA

Institute of Automatics, Faculty of Automatics, Electronics and Computer Science, Silesian University of Technology,
16 Akademicka St., 44-100 Gliwice, Poland

**Abstract.** This article presents the development of a mathematical model of a quadrotor platform and the design of a dedicated control system based on an optimal approach. It describes consecutive steps in development of equations forming the model and including all its physical aspects without commonly used simplifications. Aerodynamic phenomena, such as Vortex Ring State or blade flapping are accounted for during the modelling process. The influence of rotors' gyroscopic effect is exposed. The structure of a control system is described with an application of the optimal LQ regulator and an intuitive way of creating various flight trajectories. Simulation tests of the control system performance are conducted. Comparisons with models available in the literature are made. Based on above, conclusions are drawn about the level of insight necessary in creation of control-oriented and useable model of a quadrotor platform. New possibilities of designing and verifying models of quadrotor platforms are also discussed.

**Key words:** mathematical modelling, optimal control, quadrotor platform, autonomous flight.

## Nomenclature

$\underline{v}$ – underscore indicates that $v$ is a vector quantity,

$\underline{v}^r$ – superscript indicates that $v$ is expressed in $r$ frame components,

$\widehat{v}$ – hat indicates that $v$ is a unit vector,

$\widehat{\underline{v}}_b$ – unit vector representing $b$ frame axis,

${}^i\dfrac{d\underline{v}}{dt}$ – left superscript (derivatives only) indicates reference frame with respect to which derivative is taken,

$A$ – disc area of rotor,

B – body frame symbol,

$\underline{G}$ – torque,

$\underline{G}_{\beta,j}$ – flapping torque introduced by $j$-th rotor,

$\underline{H}$ – angular momentum,

I – inertial frame symbol,

$I$ – tensor of inertia,

$I_w$ – tensor of the rotor,

$I_s$ – combined inertia of the system composed of body and rotor treated as a point mass,

$M$ – platform's mass,

$M_w$ – rotor's mass,

P – reference frame symbol,

$R$ – rotor disc radius,

$\underline{R}$ – inertial position vector of platform's Center of Mass (CoM),

$R_w$ – distance from platform's CoM to rotor's CoM,

$\mathcal{R}_{rb}$ – transformation matrix (DCM) from $b$ to $r$ frame, indices are to be read right-to-left,

$T$ – thrust force,

$\underline{V}$ – linear velocity of platforms' CoM,

$V_c$ – climb velocity,

$V_\infty$ – freestream velocity,

$a_i$ – longitudinal flapping angle,

$\underline{g}$ – Earth's gravity acceleration,

$b, i, r, w$ – indices of body, inertial, reference and rotor frames, respectively,

$v_i$ – induced inflow velocity,

$v_h$ – induced inflow velocity in hover,

$\kappa$ – measured induced power factor in hover,

$\lambda_i$ – induced inflow ratio coefficient, $\lambda_i = v_i/(\Omega R)$,

$\theta, \varphi, \psi$ – roll, pitch and yaw orientation angle between body and reference frame, respectively,

$\rho$ – air density,

$\gamma$ – Lock number,

$\underline{\omega}_{br}$ – angular velocity of frame $r$ relative to frame $b$,

$\Omega_{bw}$ – magnitude of rotor's angular velocity in $w$ frame relative to $b$ frame.

## 1. Introduction

Quadrotor platform has been an object of scientific interest since its first successive take-off in 1920's [1]. However, even after overcoming the ground effect in 1960's [2] no particular

*e-mail: radoslaw.zawiski@polsl.pl

usage of this platform has been made only until recently. The technological progress of the last two decades, especially in sensing technologies, high density power storages and data processing enabled another version of quadrotor to come into picture.

This latest, smallest, four rotors equipped platform is making a full usage of the minimalistic modern Inertial Measurement Units (IMUs) composed of Micro Electromechanical Systems (MEMS) and inertial and magnetic sensors, such as those mentioned in [3]. It is mostly equipped with modern CPUs (especially considering their power and space requirements), GPS receivers, HD Cameras and so on. A great example of application this technology can be also found in another domain, namely biocybernetics [4]. Adding a relative simplicity in construction and maintenance of those Unmanned Aerial Vehicles (UAVs) as compared to other helicopter-like, it makes them a perfect platform for modern era research in various fields.

Among those fields are subjects from guidance, navigation and control domain, from sensors and intelligent control, from aircraft dynamics, from multi-vehicle control and many others. For most of those researches, however, there is a necessity of a usage of mathematical description of quadrotor's dynamics at some point. This description is frequently noticeably simplified. The simplifications concern platform's body dynamics as well as the aerodynamic phenomena occurring during the flight of a platform.

In the description of platform's dynamics, the most frequent simplifications are assumption of platform's symmetry [5, 6], implicit weightlessness of the rotors' blades [5–9] and the rigidity of the platform together with blades. In case of simplifications in aerodynamic description, the most common assumption is made about proportionality of rotor's thrust to the square of its angular velocity [5, 6, 8, 9]. In addition, the rotor itself is treated, according to momentum theory developed for helicopters, as an infinitely thin actuator disk. While some of those simplifications are acceptable at the early stage of development, others do not withstand the time trial and need to be released for future progress to be possible.

Considering platform's dynamics, the assumption about weightlessness of blades becomes far from reality when physical dimensions of quadrotors grow up. The same situation takes place when quadrotors are expected to perform aggressive manoeuvres and gyroscopic effects associated with the inertias of the blades become considerable. This can be observed in video materials provided by [10] and [11].

Considering platform's aerodynamics, the assumption of rotor's thrust constant proportionality to the square of its angular velocity is far from reality for every flight phase except hover. The same statement can be found in [12]. Taking into account the amount of attention put into blade flapping phenomena in helicopter analysis, it is interesting why this aspect is frequently neglected in quadrotor modelling, apart from the work described in [7, 12–16].

When designing a control system for the quadrotor platform, the most widely applied control algorithm is a PID one [5–6, 12, 14–16]. There are also successful trails of im-

plementing sliding modes [17], dynamic contraction method [18], robust and $H_\infty$ controllers [19] or optimal control [5–6]. The latter approach is of particular interest to the authors of this article, as it is also used for the control system design of the extended model presented below.

There are complications involved with every control methodology mentioned above. With the PID algorithm, for example, there are issues in terms of control quality connected with the need of change of controller's parameters depending on flight conditions in given flight phase [12] or settings dependence on physical realization of given platform [12, 14, 15]. Despite the above, PID is considered a fairly robust controller. Interestingly, the PID methodology is compared with the LQ approach in Ref. [4] and [5], based on the same mathematical model of the platform. As a result, the control system based on PID is performing better than the one based on LQ regulator. According to the authors of those articles, this is mainly due to the lack of detail in a platform's mathematical model. The model used by them is in their opinion oversimplified and hence it prevents autonomous flight under LQ regulator. Under the PID control however, the autonomous hovering is achieved due to relatively high robustness of the PID algorithm with respect to model details. A similar opinion about PID approach is stated in [14].

Given above, the question about the necessary depth of analysis of quadrotor platform and elaboration of its mathematical description is justified. In this article a detailed mathematical model of quadrotor is developed. It contains an extended description of platform's dynamics, including the inertial properties of rotors' blades, as well as extended description of aerodynamics. The thrust-to-rate proportionality is dropped for the application of fully developed momentum theory. The phenomenon of blade flapping is taken into account. For this extended model an LQ control approach is proposed and compared to the one used in [5]. Such system is then examined by simulations across different flight phases. The conclusions are drawn about the usefulness of such extended model. With all that, this article fills in the gaps in the current state of argument about justifying the simplifying assumptions made during the quadrotor dynamics modelling process. The concluding section proposes further research direction in this domain.

This paper is organized as follows: the first part (2), titled "Mathematical model development", focuses on the derivation of a useable model of quadrotor platform. It starts with the description of frames of reference, where the innovative concept of introducing additional, entirely theoretical frame called the "reference frame" (referring to the concept of "reference value" in control theory nomenclature) is explained. Then sections describing kinematics, rotational dynamics, translational motion, aerodynamics, blade flapping and actuator dynamics follow. Next major part (3) – "Control system development" – explains an idea and implementation of a dedicated control system. Consecutive part (4) describes results of simulations. It shows the simulation outcomes for hovering flight, forward flight in operator and automatic modes. This section also looks at the comparisons with other models available in

the literature and influences of disturbances. Article finishes with conclusions and suggestions of further research (5).

## 2. Mathematical model development

The development of mathematical model of quadrotor's dynamics is conceptually divided into three major parts. The first one, given in section 1 and describing the frames of reference used, is common for all later considerations. The second major part is devoted to the description of platform's body dynamics. It comprises the specific features connected with rigid body motion. This section does not consider the origin or nature of aerodynamic forces, but is rather dealing with their influence. The third major part is devoted strictly to the analysis of aerodynamic phenomena present during quadrotor operation. It includes the description and influence of thrust force and blade flapping, as well as torques resulting from them. The remaining sections complete the model and give an instruction about its implementation.

**2.1. Frames of reference.** The frames of reference used during modelling of quadrotor are shown in Fig. 1. Every frame is right-handed, with north-east-down directions. Because of the inertia tensor being constant in body frame, this frame is chosen as a main one. Additionally, the Inertial Measurement Unit (IMU) is also operating in this frame, what also supports such choice.
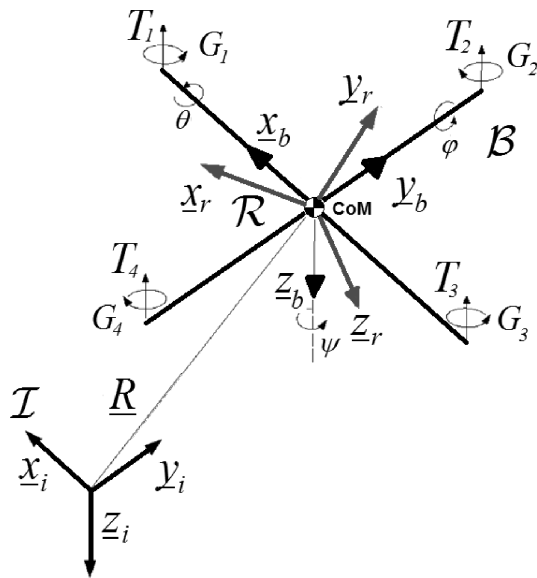


Fig. 1. Reference frames used together with principal axes, forces and moments

Let us introduce an auxiliary frame, called hereafter simply the reference frame. The origin of reference frame is in the origin of the body frame, which is in the centre of mass of platform's body. Using the reference frame the control problem can be reformulated into the minimization of misalignment between body and the reference frames, where the orientation of the latter with respect to inertial frame is known *a priori*. The interactions between reference and inertial frames

form the desired flight mode and are treated as a specific set point the control system is to follow. This also explains the name of reference frame. Such formulation of the control problem enables every attitude and trajectory desired to be regarded as a tracking problem.

**2.2. Kinematics.** The expression for linear velocity of platform's Centre of Mass (CoM) in inertial frame has the form

$$\underline{V}^i = \frac{^i d\underline{R}}{dt}. \tag{1}$$

The expression for angular velocity, which takes into account all frames of reference, has the form

$$\underline{\omega}_{bi}^b = \underline{\omega}_{br}^b + \mathcal{R}_b r \underline{\omega}_{ri}^r. \tag{2}$$

The attitude is parameterized using the Euler angles. Although there are inevitable singularities connected with this parameterization, its biggest advantage is intuitiveness in interpretation. If required, the switch to quaternion is simple and straightforward. This will be required for example when designing manoeuvres lying outside the flight envelope obtainable with Euler angles. Defining the axis – angle – name relationship as in Fig. 1, taking E123 Euler sequence for the transformation matrix $\mathcal{R}_{br}$ in Eq. (2), the body relative to reference frame rates become

$$\dot{\theta} = (\omega_{brx}^b \cos \psi - \omega_{bry}^b \sin \psi)\frac{1}{\cos \varphi},$$

$$\dot{\varphi} = \omega_{brx}^b \sin \psi + \omega_{bry}^b \cos \psi, \tag{3}$$

$$\dot{\psi} = \omega_{brz}^b - (\omega_{brx}^b \cos \psi - \omega_{bry}^b \sin \psi) \tan \varphi.$$

The superscripts for scalar values are stressing that this is the component of angular velocity vector of the body frame relative to reference frame, about given axis, expressed in body frame components.

**2.3. Rotational dynamics without momentum storage devices.** Quadrotor platform is equipped with four rotors, which store angular momentum due to their rotational motion. This is the reason of separate treatment of the angular momentum of the platform and the rotors themselves. Adding to this system external forces imposing additional torques, makes the analysis even more complicated. The detailed derivation together with in-depth discussion of the equations in this and next sections can be found in [20–21].

The angular momentum of the platform without any momentum storage devices takes the form

$$\underline{H}^i = \underline{R}^i \times \underline{v}^i M + I\omega_{bi}. \tag{4}$$

The inertial torque, given as time derivative of Eq. (4) can be written as

$$\underline{G}^i = \left( \underline{R}^i \times \frac{^i d^2 \underline{R}}{dt^2} \right) M + I\frac{^b d\underline{\omega}}{dt} + \underline{\omega}_{bi} \times (I\underline{\omega}). \tag{5}$$

In Eq. (5) two terms can be distinguished. The first one, a product of inertial position and acceleration, is resulting from inertial motion of the platform. The second one, that is the remaining terms in Eq. (5), is resulting from rotation of the platform about its CoM with respect to inertial frame and can

be seen as a gyroscopic effect from the spinning of the platform. Equation (5) is essentially the main equation describing rotational dynamics in [5, 6], [12, 14, 15]. It is clear that at this stage Eq. (5) contains no specific information about the quadrotor platform. It is rather a generic equation of a rigid body in motion across inertial space.

### 2.4. Rotational dynamics with momentum storage devices.
The inclusion of rotating rotor is depicted in Fig. 2 [20]. The angular momentum of the system comprising platform's body and rotor's body $(b + w)$ is given by

$$\underline{H}^i_{b+w} = (\underline{R} \times {}^i\underline{\dot{R}})M_{b+w} + \underline{R} \times \underline{\omega}_{bi} \times \underline{R}_w M_w$$
$$+ \underline{R}_w \times {}^i\underline{\dot{R}}M_w + \Delta I_w \underline{\omega}_{bi} + I_w \underline{\Omega}_{wi} + I\underline{\omega}_{bi}, \quad (6)$$

where the term with $\Delta I_w$ is, by parallel axis theorem, an inertia contribution of the rotor to the inertia of the platform, $\Delta I_w \underline{\omega}_{bi} = (\underline{R}_w \times \underline{\omega}_{bi} \times \underline{R}_w)M_w$. Time differentiation of Eq. (6) gives total torque acting on the system as

$$\underline{G}_{b+w} = (\underline{R} \times {}^i\underline{\ddot{R}})M_{b+w} + \frac{{}^id}{dt}(\underline{R} \times \underline{\omega}_{bi} \times \underline{R}_w M_w)$$

$$+ \frac{{}^id}{dt}(\underline{R}_w \times {}^i\underline{\dot{R}}M_w) + \frac{{}^id}{dt}(\Delta I_w \underline{\omega}_{bi}) + \frac{{}^id}{dt}(I_w \underline{\Omega}_{wi}) \quad (7)$$

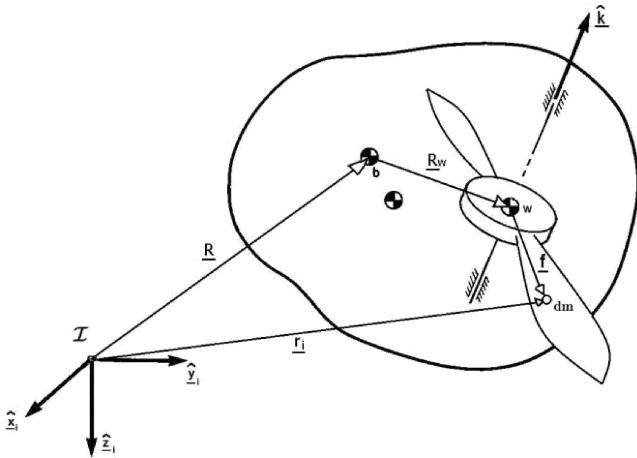$$+ \frac{{}^id}{dt}(I\underline{\omega}_{bi}).$$



Fig. 2. Geometry of quadrotor with rotor incorporated into the model

Equations (6) and (7) are genuine for any platform containing rotating elements and traveling across inertial space. For the case at hand, a set of simplifying assumption is introduced, namely

1. CoM of the body is inertially fixed, resulting in $\underline{R}$ = const;
2. CoM of the body is in the origin of the inertial frame, hence $\underline{R} = 0$.

In simplified form, Eq. (7) takes the form

$$\underline{G} = \frac{{}^id}{dt}(I_s \underline{\omega}_{bi} + I_w \underline{\Omega}_{wi}). \quad (8)$$

After proper decomposing of rates in Eq. (8), it becomes

$$\underline{G} = (I_s + I_w)^r\underline{\dot{\omega}}_{ri} + (I_s + I_w)^b\underline{\dot{\omega}}_{br} + I_w{}^b\underline{\dot{\Omega}}_{wb}$$

$$+ W_{ri}(I_s + I_w)\underline{\omega}_{ri} + (W_{ri} + W_{br})(I_s + I_w)\underline{\omega}_{br} \quad (9)$$

$$+ (W_{ri} + W_{br})I_w\underline{\Omega}_{wb},$$

where and $\underline{\omega} \times \underline{x} = W\underline{x}$ and $W$ is a matrix composed of elements of $\underline{\omega}$, and $\underline{x}$ is any appropriate vector. For Eq. (9) to convey information about internal placement of rotor, its angular velocity is presented as

$$\underline{\Omega}^b_{wb} = \Omega_{wb}\widehat{\underline{k}}^b, \quad (10)$$

where $\underline{k}$ is a direction vector of the rotor's spin axis in the body frame, as in see Fig. 2. Quadrotor contains four rotors grouped into counter-rotating pairs, which differ only in the direction of rotor's spin vector (see Fig. 1). Aligning the spin axes with vertical principal axis of the platform, the following assignment takes place: pair $(1, 3) \rightarrow -\underline{k}_3 = [0\ 0\ -1]$; pair $(2, 4) \rightarrow \underline{k}_3 = [0\ 0\ 1]$, where $\underline{k}_3$ is a unit vector in the direction of $\underline{z}_b$ axis in body frame. This enables proper expansion of Eq. (9) by means of Eq. (10).

### 2.5. Influence of aerodynamic forces on rigid body dynamics.
The total torque coming from, say, rotor 1, expressed in inertial frame, is a vector sum of the form

$$\underline{G}_{w,1} = \underline{G}'_{w,1} + \underline{G}''_{w,1}. \quad (11)$$

The first component in Eq. (11) results from rotor's rotational motion. The second component results from the rotor-produced thrust force. Similarly to Eq. (9), taking first derivative expressed with respect to reference frame and the two latter with respect to body frame, the first component of Eq. (11) becomes

$$\underline{G}'_{w,1} = I_w{}^r\underline{\ddot{\omega}}_{ri} + I_w{}^b\underline{\dot{\omega}}_{br} + I_w{}^b\underline{\dot{\Omega}}_{wb} + W_{ri}I_w\underline{\omega}_{ri}$$
$$+ (W_{ri} + W_{br})I_w\underline{\omega}_{br} + (W_{ri} + W_{br})I_w\underline{\Omega}_{wb}. \quad (12)$$

The second component in Eq. (11) is of aerodynamic origin. It represents the torque coming from the thrust force created by the airflow through the rotor's disk and associated flapping effect. Suppose that the projection of thrust force produced by the $j$-th rotor on the $\underline{z}_b$ axis in body frame is $\underline{T}_j$. Hence, from geometry of Fig. 2 and axes assignment

$$\underline{G}''_{w,1} = -\mathcal{R}_{ir}\mathcal{R}_{rb}(\widehat{\underline{k}}_1 R_w \times \widehat{\underline{k}}_3 T_1) + \underline{G}^i_{\beta,1}. \quad (13)$$

The net torque acting on a platform's body differs from the one given by Eq. (8) by the terms representing thrust and drag. Thus the extended form

$$\underline{G} = \frac{{}^id}{dt}(I_s\underline{\omega}_{bi} + I_w\underline{\Omega}_{wi}) + \sum_{j=1}^{4}\underline{r}^i_j \times \underline{T}^i_j + \underline{G}^i_\beta + \underline{D}^i_r, \quad (14)$$

where the last term is related to aerodynamic drag. To obtain the total torque from Eq. (14) in body frame, that is in the frame controller is operating, appropriate transformation is performed. The resulting equation is marked (15). Equation (16) clearly shows the influence of wheel's inertia. It can be easily quantified for given quadrotor setup and its importance compared to other elements present in this equation.

This is an element frequently missing in an up-to-date treatment of quadrotor modelling, as stated in the introductory part.

Summing up, rotational dynamics of quadrotor can be put into one equation comprising the general torque acting on the system (16) and individual torques originating from every rotor in the form of Eq. (11). In order to preserve readable content, such equation will have the form

$$
\begin{bmatrix} \underline{G}^b \\ \underline{G}_1^b \\ \underline{G}_2^b \\ \underline{G}_3^b \\ \underline{G}_4^b \end{bmatrix} = f_r({}^r\underline{\dot{\omega}}_{ri}, {}^b\underline{\dot{\omega}}_{br}, {}^b\underline{\dot{\Omega}}_{1-4}, \underline{\omega}_{ri}, \underline{\omega}_{br}, \Omega_{1-4}, T_{1-4}, \underline{G}^b_{\beta,1-4}),
$$

(15)

$$
\underline{G}^b = (\mathcal{R}_{ir}\mathcal{R}_{rb})^{-1} \left\{ (I_s + 4I_w)^r\underline{\dot{\omega}}_{ri} + (I_s + 4I_w)^b\underline{\dot{\omega}}_{br} \right.
$$

$$
\left. + I_w[-\hat{\underline{k}}_3 \ \hat{\underline{k}}_3 \ -\hat{\underline{k}}_3 \ ; \ \hat{\underline{k}}_3] \begin{bmatrix} {}^b\dot{\Omega}_1 \\ {}^b\dot{\Omega}_2 \\ {}^b\dot{\Omega}_3 \\ {}^b\dot{\Omega}_4 \end{bmatrix} \right\}
$$

$$
+ (\mathcal{R}_{ir}\mathcal{R}_{rb})^{-1} \left\{ W_{ri}(I_s+4I_w)\underline{\omega}_{ri} + (W_{ri}+W_{br})(I_s+4I_w)\underline{\omega}_{br} \right.
$$

$$
\left. + (W_{ri} + W_{br})I_w[-\hat{\underline{k}}_3 \ \hat{\underline{k}}_3 \ -\hat{\underline{k}}_3 \ ; \ \hat{\underline{k}}_3] \begin{bmatrix} \Omega_1 \\ \Omega_2 \\ \Omega_3 \\ \Omega_4 \end{bmatrix} \right\}
$$

$$
+ [-(\hat{\underline{k}}_1 R_w \times \hat{\underline{k}}_3 T_1) - (\hat{\underline{k}}_2 R_w \times \hat{\underline{k}}_3 T_2)
$$

$$
+ (\hat{\underline{k}}_1 R_w \times \hat{\underline{k}}_3 T_3) + (\hat{\underline{k}}_2 R_w \times \hat{\underline{k}}_3 T_4)] + \underline{G}^b_\alpha + D_r^b,
$$

(16)

where $f_r$ is a function of appropriate variables. The arguments of $f_r$ such as $\Omega_{1-4}$ are to be read $\Omega_{1-4} := \{\Omega_1, \Omega_2, \Omega_3, \Omega_4\}$. It is important to notice, that the left hand side of Eq. (15) contains also environmental disturbances and aerodynamic drag, which are hidden under the term $\underline{G}$.

**2.6. Translational motion.** The inertial net force acting on the body is composed of gravity and thrust with direction and magnitude dependent on an instantaneous orientation of the platform with respect to inertial frame and operational conditions of rotors. Let us introduce the notion of

$$
\underline{T}_c := \sum_{j=1}^4 \underline{T}_j
$$

(17)

which defines a vector sum being the total thrust produced by rotors, taken about platform's centre of mass. The linear acceleration of platform is than

$$
\frac{{}^i d\underline{V}}{dt} = \underline{g} - \frac{1}{M}\mathcal{R}_{ir}\mathcal{R}_{rb}\underline{T}_c^b + \frac{1}{M}\underline{D}_t,
$$

(18)

where $\underline{D}_t$ is aerodynamic translational drag force.

**2.7. Aerodynamics of flight.** In the description of aerodynamics, the airflow is described under classical assumptions for the momentum theory, as considered in helicopter analysis [1]. The airflow is steady, incompressible, inviscid and quasi one-dimensional. The last assumption means that mostly only vertical component of the airflow through rotor's disc plays important part. Basic assumption concerning the rotor itself is that it is infinitely thin actuator disc (as for thrust generation). Similar approach is also widely applied in previous work on this subject. However, as stated in the introduction, in this article momentum theory is used consequently in full extent to cover all flight phases. Additionally, elements of blade element theory are applied for the description of flapping.

In the simple case of axial flight, where only vertical motion is considered, the conditional equation for thrust is derived from conservation of mass flow and its momentum, as can be found in [1, 22] and other classical books on helicopter aerodynamics. This conditional equation is

$$
T = \begin{cases} 2\rho A(V_c + v_i)v_i & \text{if} \quad V_c > 0 \\ 2\rho A v_i^2 & \text{if} \quad V_c = 0 \\ -2\rho A(V_c + v_i)v_i & \text{if} \quad V_c \leq -2v_h \end{cases}
$$

(19)

Equation (19) shows, that using the definition of induced inflow ratio coefficient, $\lambda_i = v_i/(\Omega R)$, thrust can be treated as constantly proportional to the square of rotor's angular velocity, but only in hovering flight.

The region not covered by Eq. (19), where the method of derivation of Eq. (19) is invalid, is called the Vortex Ring State (VRS). This situation is dealt with by applying empirically found coefficients, by means of which the thrust curve is fitted to the measurements and elongated in continuous manner. This results in the following equation

$$
\frac{v_i}{v_h} = \begin{cases} -\frac{V_c}{2v_h} + \left(\left(\frac{V_c}{2v_h}\right)^2 + 1\right)^{1/2} \\ \kappa + k_1\left(\frac{V_c}{v_h}\right) + k_2\left(\frac{V_c}{v_h}\right)^2 + k_3\left(\frac{V_c}{v_h}\right)^3 + k_4\left(\frac{V_c}{v_h}\right)^4 \\ -\frac{V_c}{2v_h} - \left(\left(\frac{V_c}{2v_h}\right)^2 - 1\right)^{1/2} \end{cases}
$$

(20)

where $V_c > 0$ in the first case, $0 > V_c \geq -2v_h$ in the second case and $V_c \leq -2v_h$ in the third one. The constants are $k_1 = -1.125$, $k_2 = -1.372$, $k_3 = -1.718$ and $k_4 = -0.655$ and the average value of $\kappa$ may be taken as 1.15 for preliminary design [1].

In more general case of forward flight, the symmetry of flow is lost and one has to additionally consider the freestream velocity $V_\infty$ of the air relative to each of the rotors. The thrust force in this case for given rotor is given by (rotor's index omitted for clarity)

$$T = 2\rho A v_i ((V_\infty \cos\alpha)^2 + (V_\infty \sin\alpha + v_i)^2)^{1/2}, \quad (21)$$

where $\alpha$ is rotor's disk angle of attack. Introducing tip speed ratio coefficient $\mu = V_\infty \cos\alpha / (\Omega R)$ the induced inflow ratio becomes

$$\lambda = \mu \tan\alpha + \frac{\lambda_h}{(\mu^2 + \lambda^2)^{1/2}} + \lambda_c \cos\alpha, \quad (22)$$

where $\lambda_c = V_c/(\Omega R)$ and index $h$ stands for hover state. From Eq. (22) it is straightforward to numerically obtain inflow velocity and, in consequence, thrust force for each type of flight. However, according to [1], a nonphysical solution will always be obtained if there is a descent (upward) component of the velocity normal to the rotor disk which is between 0 and $2v_h$. Hence, when the rotor is operating in a VRS type conditions, caution should be paid. The numerical algorithms can behave in various ways, so a cross-check should be applied wherever possible.

**2.8. Blade flapping.** The phenomenon of blade flapping is strictly connected with rotating nature of rotor's blades. Blade flapping was recognized as an important factor influencing stability and control performance [12, 14]. A derivation of dependence between flapping angles and helicopter flight properties is shown e.g. in [1] or [22, 23]. Following the derivation in [22], it can be shown that for fixed pitch blades of quadrotor with linear twist the first harmonic approximation of longitudinal flapping angle in steady level flight is

$$a_{1s} = \frac{\frac{8}{3}\theta_0\mu + 2\theta_1\mu\left(\mu\alpha_s - \dfrac{C_T}{\sigma\frac{\mu^2}{2}}\right)}{1 - \dfrac{\mu^2}{2}}$$

$$+ \frac{12\dfrac{e}{R}}{\gamma\left(1-\dfrac{e}{R}\right)^3\left(1-\dfrac{\mu^4}{4}\right)}\left[\frac{C_T}{\sigma}\left(\frac{\frac{8\mu\gamma}{9C_{l_\alpha}}\left(1-\dfrac{e}{R}\right)^2}{1+\dfrac{e}{2R}} + \frac{\sigma}{2\mu}\right)\right], \quad (23)$$

where $\gamma = \rho C_{l\infty} c R^4 / I_b$ is a Lock number, $e$ is a blade hinge offset, $\theta_0$ and $\theta_1$ are blade linear twist coefficients, $\sigma = A_{blades}/A_{rotor}$ is called rotor solidity and $C_T$ is a rotor thrust coefficient. During pitching and rolling motion of the platform Eq. (23) needs to be extended by a component related to pitch $q$ and roll $p$ platform velocities giving

$$a_{1s} = (23) + \frac{\dfrac{-16}{\gamma}\left(\dfrac{q}{\Omega}\right)}{\left(1-\dfrac{e}{R}\right)^2} + \dfrac{p}{\Omega}}{1 - \dfrac{\mu^2}{2}}$$

$$+ \frac{\dfrac{12e}{\gamma R}}{\left(\dfrac{1-e}{R}\right)^3}\left[\dfrac{-\dfrac{16}{\gamma}\left(\dfrac{p}{\Omega}\right)}{\left(\dfrac{1-e}{R}\right)^2} - \dfrac{q}{\Omega}\right]}{1 - \dfrac{\mu^4}{4}} \quad (24)$$

The lateral flapping was neglected in above considerations, as due to quadrotor's symmetry and in-pair counter rotations of rotors its net influence is negligibly small in all instances of forward flight. Having flapping angle given above, expression of flapping torque in vector notation for $j$-th rotor takes the form

$$\underline{G}_{\beta,j}^b = -\frac{dM_M}{da_{1s_j}}a_{1s_j}\widehat{\underline{V}}_{ip} \times \widehat{\underline{k}}_3$$

$$+ h_M(Ta_{1s_j} + H_{a_{1s_j}=0})\widehat{\underline{k}}_3 \times \widehat{\underline{V}}, \quad (25)$$

where $\underline{V}_{ip}$ is a projection of a unit vector in the direction of platforms' linear inertial velocity expressed in body frame onto the $(\underline{k}_1, \underline{k}_2)$ plane, $H$ is a rotor in-plane force, $h_M$ and $l_M$ are vertical and horizontal distances from CoM to rotor hub and $M_M$ is the total rotor moment in pitch direction. Its $a_{1s}$ – derivative, under the assumption of uniform blade mass distribution is

$$\frac{dM_M}{da_{1s}} = \frac{3}{4}\left(\frac{e}{R}\right)\frac{A_{N_b}C_{l_\alpha}\rho(\Omega R)^2 R}{\gamma}, \quad (26)$$

where $A_{Nb}$ is the total area of $N_b$ blades, $C_{l_\alpha}$ is a 2D blade aerofoil lift-curve-slope. The geometry of the problem is presented in Fig. 3.
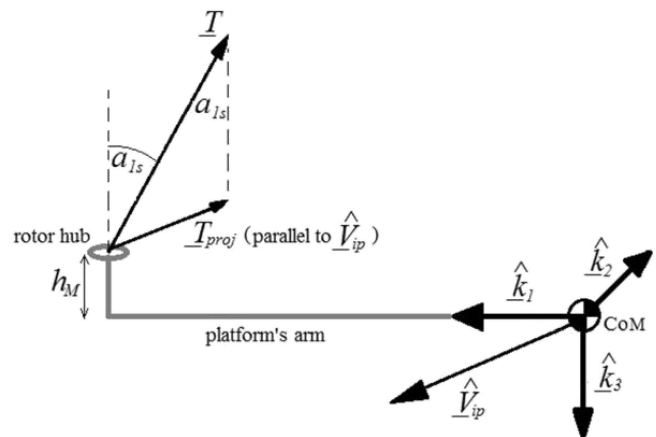


Fig. 3. Thrust vector deflection caused by flapping

**2.9. Complete model of dynamics.** Above equations for kinematics (1), (3), body dynamics (15), (18), and aerodynamics (21), (25) give a complete model of quadrotor's behaviour.

It includes both, the influence of blades' inertias with associated gyroscopic effects as well as flapping torques. In that matter it is an extension as compared to work in [5–9, 12]. Having all phases of flight described by means of momentum theory it is possible to introduce appropriate switching during simulation so as to obtain best possible approximation of rotor thrust. Such approach is much closer to reality than stiff assumption about thrust-to-square-rate proportionality, as assumed in [5–9].

**2.10. Actuators dynamics.** To complete the model of quadrotor's dynamics the description of actuators needs to be included. The motor selected is a brushless direct current (BLDC) electrical unit, what is similar to [5–6, 12, 14, 15]. The detailed description and model derivation for a standard BLDC, applicable in Matlab/Simulink environment, can be found in [24]. However, for the purpose of this work, a simplified model of BLDC motor is used. Those simplifications are similar to the ones applied and experiment-validated [12]. The description follows the one in [25].

The rotor power manifested on the shaft is given by

$$P_{shaft} = G_m \Omega_m. \tag{27}$$

Assuming that the blades of the $j$-th rotor are mounted directly on the motor shaft, and that the shaft's axis of rotation is collinear with rotor's axis of rotation, the angular velocity of the shaft is equal to the angular velocity of the rotor, $\Omega_{m,j} = \Omega_j$. The $j$-th motor torque $G_{m,j}$ is then given by

$$G_{(m,j)} = \left( \left( v_{m,j} - \frac{\Omega_j}{K_V} \right) \frac{1}{R_m} - i_0 \right) \frac{1}{K_Q}, \tag{28}$$

where $K_Q$ is a motor specific torque constant, $i_0$ is a zero-load current, $R_m$ is internal resistance of the motor, $K_V$ is a motor specific speed constant. All motor units are the same. Equation (28) is a basic equation which is applicable and describes the behaviour of actuators.

## 3. Control system development

Analysis of equations forming the model is an important stage during selection of a controller. From the structure of mentioned equations it is obvious that the system at hand is a MIMO one. Furthermore, it is already described in the state space form. For the state vector $x$ defined as

$$\underline{x} := [\underline{x}_{ang}, \underline{x}_{rot}, \underline{x}_{pos}],$$

$$\underline{x}_{ang} = [\theta, \varphi, \psi, \underline{\omega}_{br}],$$

$$\underline{x}_{rot} = [\Omega_1, \Omega_2, \Omega_3, \Omega_4], \tag{29}$$

$$\underline{x}_{pos} = [\underline{R}, \underline{V}]$$

it may be possible to obtain measurements of all state variables. Scope of this work and hence interest in controller design is limited to some of possible flight phases. We are not taking into account the take-off or landing phases, as specific aerodynamic phenomena occurring then require separate

treatment in terms of modelling [1]. A similar situation is when considering aggressive manoeuvres like flips. For all remaining flight phases it was proven by preceding experimental work in this field that linear approximation of quadrotor platform resembles well enough a real system. That allows a choice of controller among those created for linear systems, ranging from classical PID control to fuzzy logic [26]. However, all of above justifies the choice of developing a well-known LQ controller with infinite horizon as a basic controller in this work, especially taking into account how little attention is put to this control methodology in quadrotor literature. What is more, this type of controller is still being developed [27], what enables further improvements in the field of its applications.

The working point $\underline{x}_0$ about which the system is linearized for LQR implementation is in fact a given flight phase. An example of it is a hover case

$$\underline{x}_{0h} := [\underline{x}_{ang}, \underline{x}_{rot}, \underline{x}_{pos}],$$

$$\underline{x}_{ang} = [0, 0, 0, 0, 0, 0],$$

$$\underline{x}_{rot} = [\Omega_{1h}, \Omega_{2h}, \Omega_{3h}, \Omega_{4h}], \tag{30}$$

$$\underline{x}_{pos} = [\underline{R}_h, 0, 0, 0],$$

where first three entries in $\underline{x}_{0h}$ denote alignment between body and reference frame; entries four to six denote no rotation between reference and body frame; entries seven to ten denote the rotational velocity of rotors in hover; entries eleven to thirteen under $\underline{R}_h$ denote inertial coordinates of platform's CoM; entries fourteen to sixteen denote no inertial movement of platform's CoM. The system diagram is given in Fig. 4. One can notice clear separation of platform's dynamics and aerodynamics, what is consistent with above analysis.
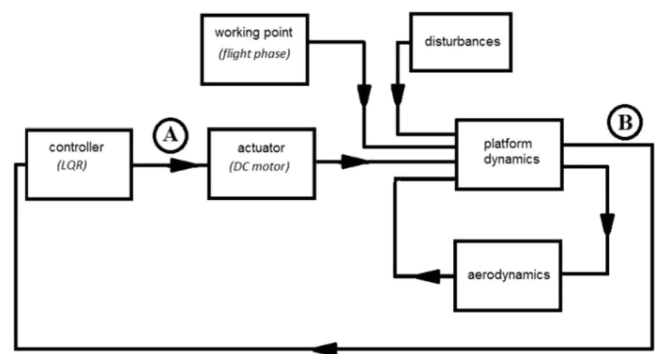


Fig. 4. Schematic of a control system, where part between A and B is linearized for LQR design

**3.1. Controller's synthesis.** For implementation of the LQ controller linearization about the working point $\underline{x}_0$ has to be performed. In general, the procedure of controller synthesis may be summarized in the following steps:

1. Choose given flight phase (i.e. select working point $\underline{x}_0$);
2. linearize about given working point $\underline{x}_0$;
3. set values for $Q$ and $R$ and obtain optimal gain $K$.

Above approach is in fact a specific form of gain schedul-ing, where the "switching" is dependent on a particular flight trajectory the system is to follow.

The linearization process is based on numerical perturba-tion around a set working point and is performed by a Mat-lab/Simulink software. The points between which system is linearized (disregarding disturbances) are marked as A and B in Fig. 4. It is important to notice that they include al-so the actuators. After linearization, system's dynamics are described by

$$\dot{\underline{x}} = A\underline{x} + B\underline{u}, \qquad (31)$$

where $A$ and $B$ are constant matrices. The control signal $\underline{u}$ is composed of control voltages which are applied to the mo-tors. This makes the implementation of an LQR algorithm with infinite horizon a straightforward task.

**3.2. Flight modes.** When designing a control system, two modes of flight are analysed. The first one, labelled as oper-ator mode and the second one, labelled as automatic mode. The concept of operator flight is to align operator's joystick from RC controller with a reference frame (see Fig. 1). Reg-ulator is then forced to align body and reference frames. In that way a simple control mechanism is created, where most of the classical helicopter pilot's tasks are performed by the regulator.

The idea of the automatic flight mode is simply to force the platform to follow a predefined inertial trajectory. This trajectory needs to be decomposed into consecutive operating points and inertial-reference frames interactions, as described with the hover example. Such approach leads to a control sys-tem composed of two levels. The upper level is responsible for decomposition of a user-defined trajectory, while the low-er level is responsible for driving the platform to the working point delivered by the upper level system.

## 4. Simulations' results

The simulations below are performed with the usage of Mat-lab/Simulink software. For the simplicity it was assumed in all sections below that platform's centre of pressure is coincident with its centre of mass. As this assumption is frequently an oversimplification in aerodynamic studies, it is believed that at this stage of control system design it is acceptable to asses control system capabilities upon it. See also discussion in [20, 28, 29]. Table 1 gives the values of physical parameters used for simulation. Figure 5 presents the conceptual drawing of a quadrotor we simulate. It is adapted from [30], an article by other members of our faculty engaged in physical realisa-tion and analysis of classical control algorithms for the same platform.

Table 1
Physical parameters used in simulation

| physical constants | | |
|---|---|---|
| quadrotor's total mass | 1 | kg |
| quadrotor's moment of inertia about its CoM | $10^{(-4)} \cdot \mathrm{diag}\,175, 175, 300$ | kg m$^2$ |
| geometrical constants | | |
| distance from paltform's CoM to rotor's shaft | 0.3 | m |
| rotor's radius | 0.15 | m |
| vertical distance from rotor's CoM to platform's CoM | 0.03 | m |
| motor constants | | |
| motor speed constant | 115 | rad/s/V |
| motor torque constant | 120 | A/N/m |
| motor internal resistance | 0.26 | Ohm |
| motor zero-load current | 0.35 | A |
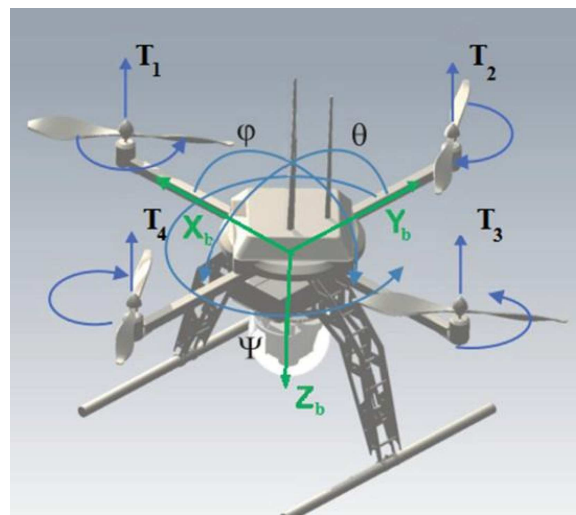


Fig. 5. Conceptual drawing of a simulated quadrotor

**4.1. Hovering flight.** Having a working point defined by (30) and setting $R_{ri}$ to be an identity matrix, a test with initial 20 degrees misalignment in every axis was performed. Controller is forced to control attitude as well as inertial position of the platform.

The results of tests performed on full nonlinear model are shown in Fig. 6 and 7. Controller performs very well, as it is able to stabilise both, attitude and position in relatively short time. Additionally, position is not only stabilized in the sense that it is not changing, but controller is able to force the plat-form to maintain itself in a specified inertial spot. This is a considerable improvement when comparing to previous work in the field, notably [5], where only attitude control realisation was considered with the usage of LQR.
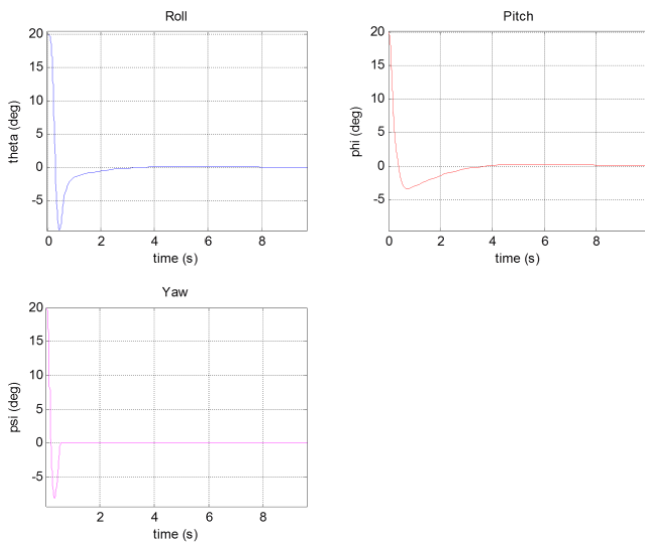
Fig. 6. Attitude angles evolution of hover flight with initial 20 degrees misalignment in every axis
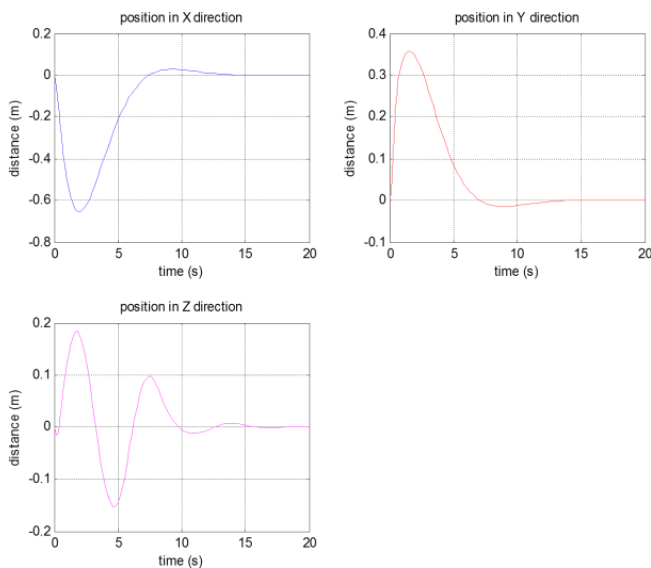


Fig. 7. Inertial position in X, Y and Z axes for hover test with 20 degrees initial misalignment

**4.2. Forward flight in operator mode.** In terms of hovering flight, the extended quadrotor model developed in this article and the simplified models mentioned in multiple references are reduced to essentially the same set of equations. For this reason it is important to examine the extended model derived here together with the control system in other flight phases, notably in forward flight.

Figure 8 presents the operator commanded input, that is the orientation angles time history between inertial and reference frames. As the role of the controller is to align body and reference frames, those operator inputs are forcing forward flight of the platform.

It is important to mention, that operator is using only cyclic stick (responsible for pitch and roll control) without touching collective lever (responsible for total thrust). The controller itself is responsible for maintaining all other flight parameters unchanged. After sixth second operator uses a predefined 'stop' command, forcing the platform to stop. The time history of inertial position and velocity is given in Fig. 9. It shows that the controller is operating almost as expected. It is enough for the operator to use "cyclic stick" to fly forward, as the "collective lever" action is in fact performed by the controller. This is certainly a great simplification in terms of acquiring necessary skills to pilot the platform. With intended motion only in $X$ direction, after about 7 meters the displacement in $Y$ direction is less than $5 \cdot 10^{-3}$ m, which is a negligible value.

Unfortunately the displacement in $Z$ direction, resulting from forward flight only (first six seconds in Fig. 9) is about 0.1 m, what might be a considerable issue. Additionally, after initiating
hover flight, there was a steady state error in both, $Y$ and $Z$ channels. In search of solution to this problem the integral action was implemented in "position in Z direction" channel into the LQR algorithm. With an integral action in the vertical inertial position channel, controller is capable of reducing steady state error. Because of relative simplicity of controller's modification, the integration action can be applied to more channels if necessary.

Another aspect of quadrotor behaviour, visible in Fig. 9, is of crucial importance. Namely, when transitioning from hover to forward flight there is an upward motion of the platform. This is a fundamental characteristic of a helicopter, examined in much detail in literature devoted to helicopter aerodynamics [1, 31]. This phenomenon originates in the excess power available when transitioning from hover to forward flight. Unless any significant acceleration is involved, rotors lift is equal to platform weight and platform climbs by virtue of excess power available. It needs to be noticed that it is impossible to see this phenomenon if thrust is assumed strictly proportional to square of rotors angular velocity, as is done e.g. in Ref. [5–8, 13]. This phenomenon is closely inspected in "Importance of model elements" section. As foreseeing such behaviour might be critically important, especially for indoor inspection missions, this constitutes another reason for, and justifies, development of the model described in this article.
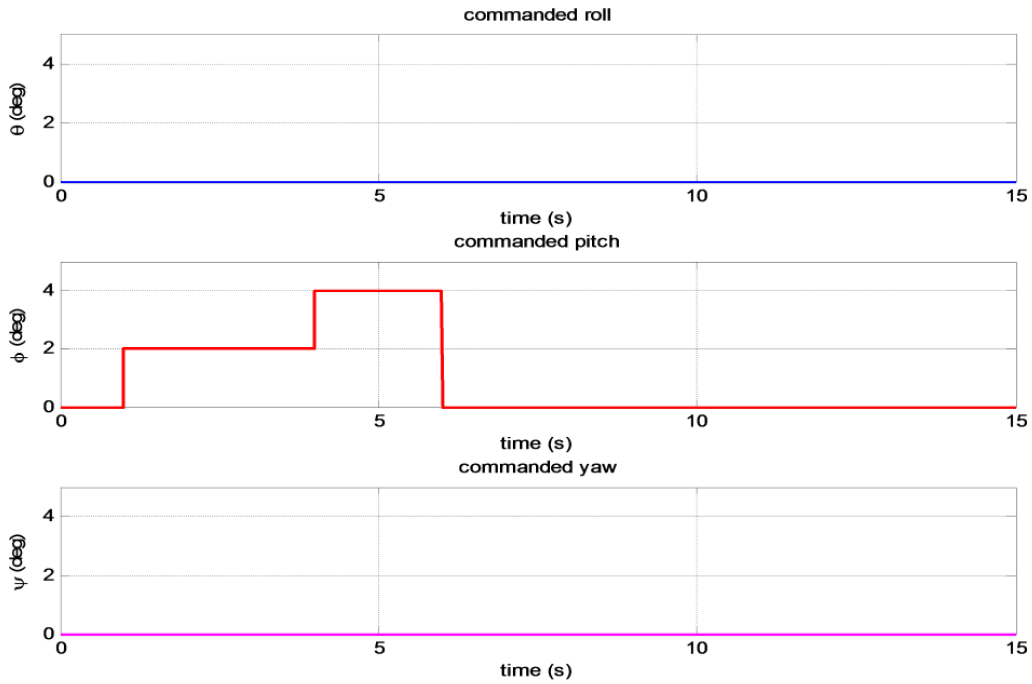
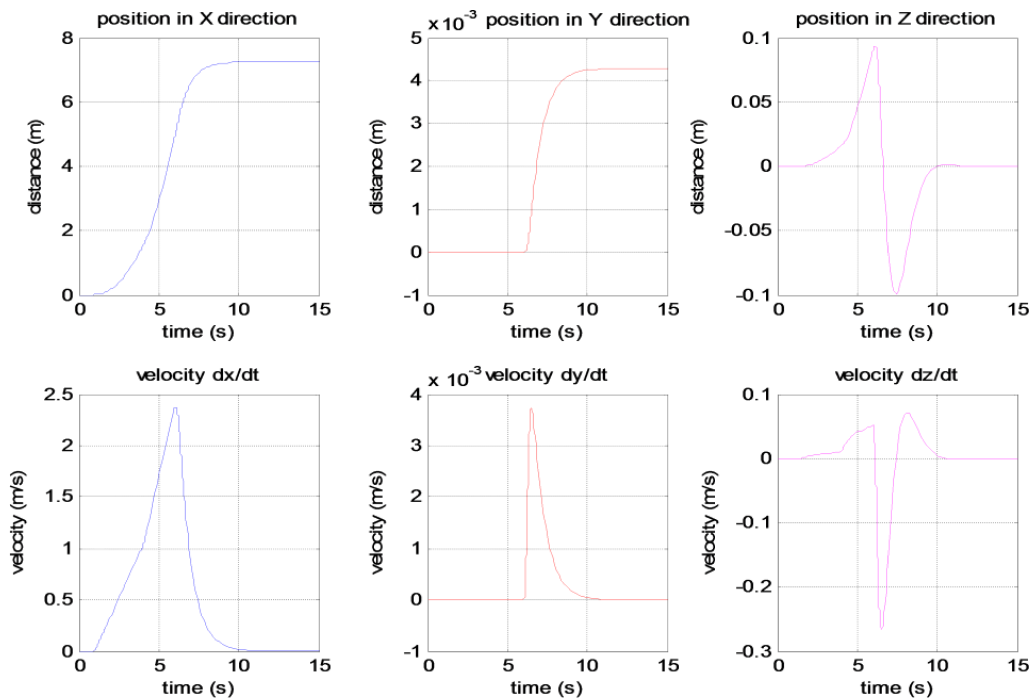Fig. 8. Operator commanded inputs for roll, pitch and yaw angle



Fig. 9. Inertial position and velocity for operator commanded inputs when regulator is implemented with integral action in "position in $Z$ direction" channel

**4.3. Forward flight in automatic mode.** The automatic forward flight test shows the results for flight with a predefined trajectory. Platform, being initially at hover, is supposed to cover distance of 10 m in $X$ direction with velocity of 1 m/s, then change to 2 m/s again in $X$ direction, simultaneously climbing in $Z$ direction with the velocity of 1 m/s. After covering total horizontal distance of 30 m it is to perform a stop manoeuvre. Figure 10 shows designed velocity profile and system response versus inertial displacement. Figure 11 shows time evolution for the same variables. Regulator again performs very well, there are no significant overshoots and the response is very quick. It needs to be pointed out, however, that in order to prevent steady state error an integral action was again introduced into controller to every velocity channel.
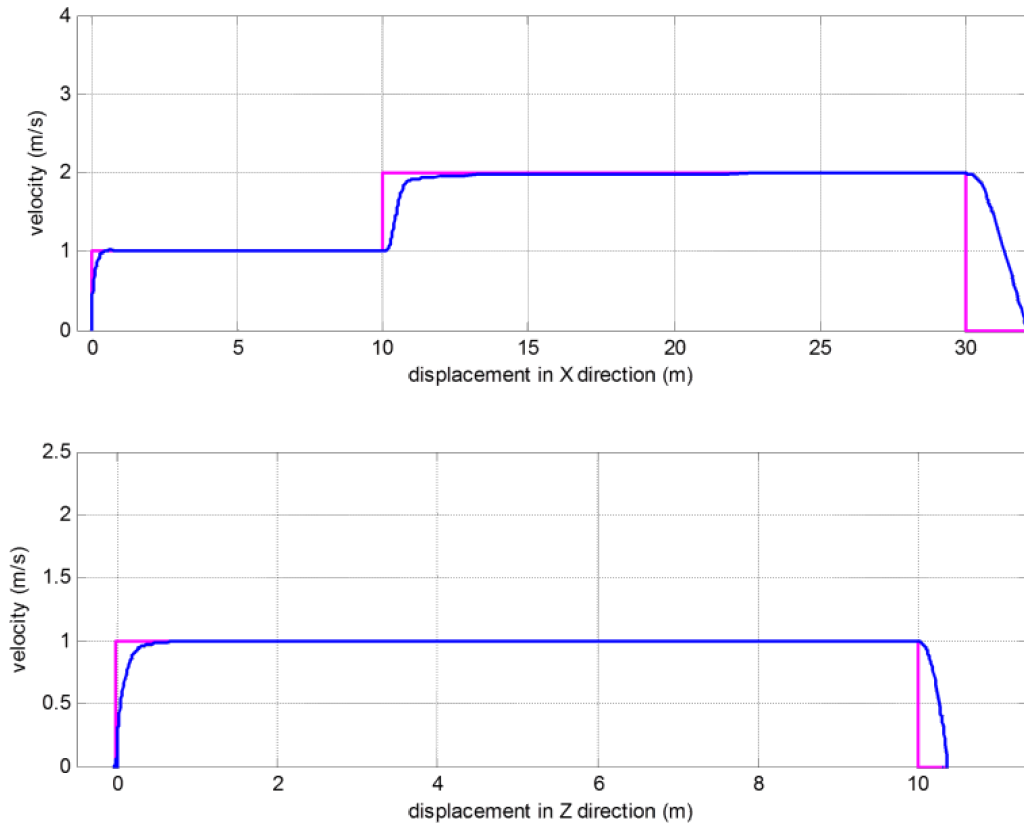
Fig. 10. Commanded velocity profile (violet) and system response (blue) for $X$ direction (upper) and $Z$ direction (lower picture)
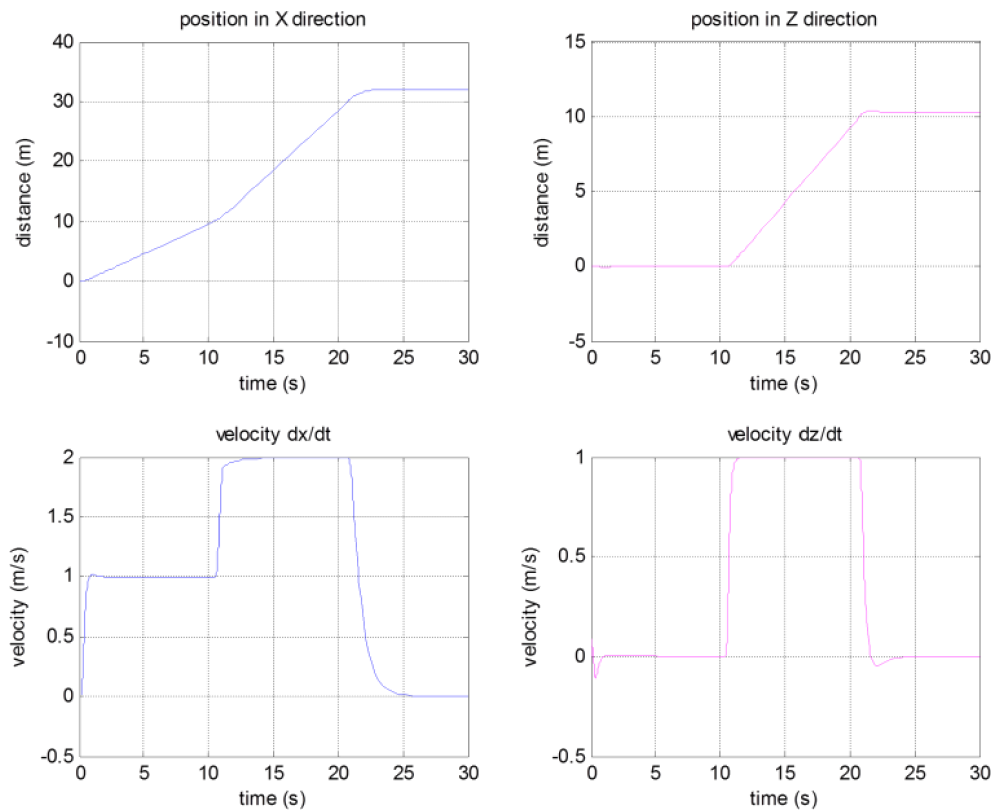


Fig. 11. Time history of system response for $X$ and $Z$ direction with a predefined trajectory

For that test system was linearized around three operating points, namely

$$\underline{x}_{01} := [\underline{x}_{ang}, \underline{x}_{rot}, \underline{x}_{pos}],$$

$$\underline{x}_{ang} = [0, \varphi_{var}, 0, 0, \omega_{yvar}, 0]),$$

$$\underline{x}_{rot} = [\Omega_{1var}, \Omega_{2var}, \Omega_{3var}, \Omega_{4var}], \quad (32)$$

$$\underline{x}_{pos} = [R_{xvar}, 0, 0, 1, 0, 0],$$

$$\underline{x}_{02} := [\underline{x}_{ang}, \underline{x}_{rot}, \underline{x}_{pos}],$$

$$\underline{x}_{ang} = [0, \varphi_{var}, 0, 0, \omega_{yvar}, 0]),$$

$$\underline{x}_{rot} = [\Omega_{1var}, \Omega_{2var}, \Omega_{3var}, \Omega_{4var}], \quad (33)$$

$$\underline{x}_{pos} = [R_{xvar}, 0, R_{zvar}, 2, 0, -1],$$

and (30). The entries with index *var* denote state variables that are not supposed to be in steady state. Results of this simulation test are very promising, as they allow a simple composition of more sophisticated trajectories, such as circular or spiral one. For that purpose it is enough to operate on working points similar to defined above and on interactions between inertial and reference frames, as controller tries at each time to align body and reference frames.

An example of such approach is shown in Fig. 12. The platform is supposed to flight upward in a spiral-like trajectory. In the simplest version presented in Fig. 12, this trajectory is approximated by means of linearization around working point similar to (33) and rotations of (initially aligned) reference frame with respect to inertial frame around the direction of $\underline{z}_i$ by 60 deg. consecutively after appropriate time period.
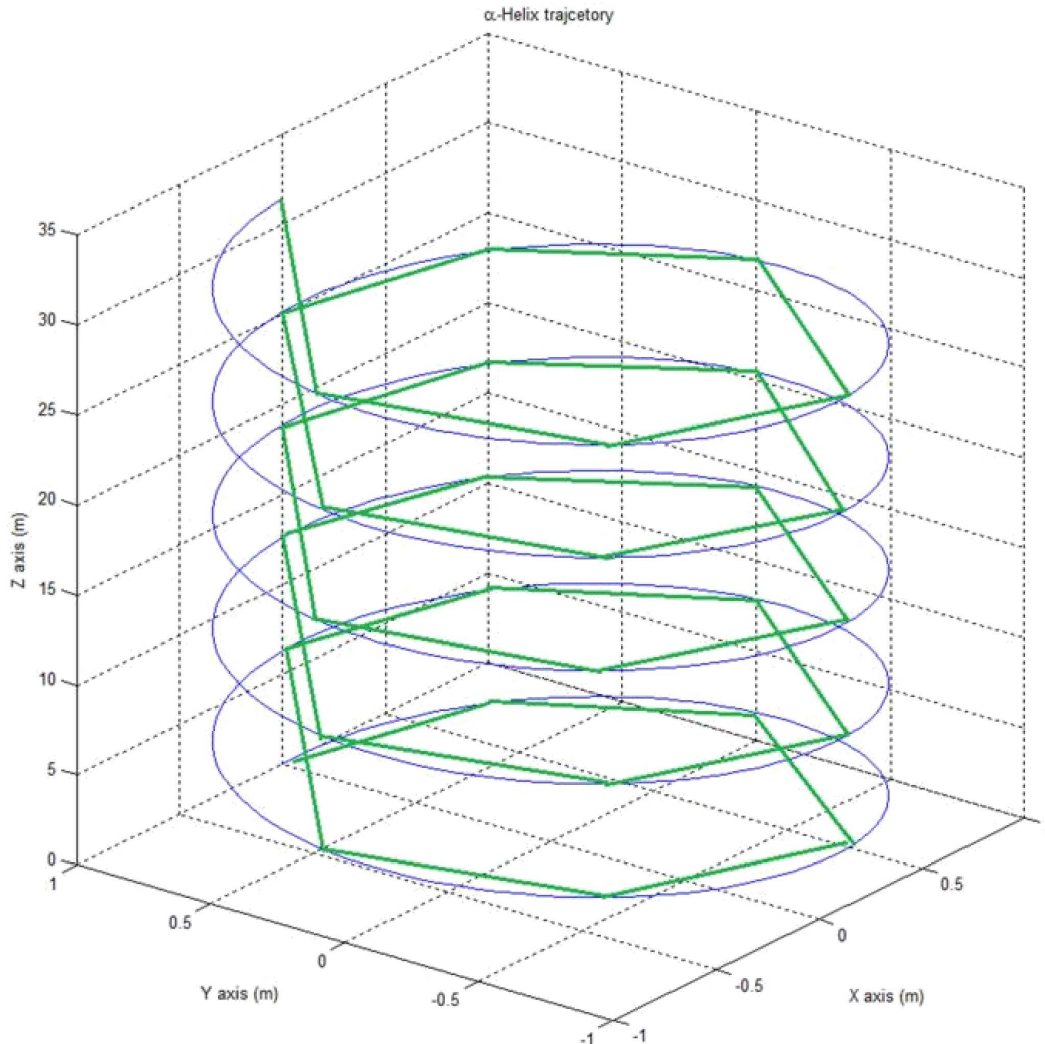


Fig. 12. An alpha-helix (spiral) trajectory of platform's CoM (blue) with its approximation (green). It is a great example where the innovative approach of introducing additional reference frame brings benefits. Green trajectory above is obtained using only one working point, the system is linearized about, and rotations of reference frame with respect to inertial frame by given angle in specified time intervals

**4.4. Comparison tests.** This part focuses on comparison tests between the model and control system developed in this article and the ones presented [5, 12, 13], or [32]. This is because the work performed by those particular groups of scientists is frequently cited in articles concerning quadrotors and their optimal attitude control. The authors in [5] and [32] are not able to obtain autonomous hover on the basis of their model and LQ controller design. They state that this situation is partially resulting from poor model quality, but do not investigate it further. After obtaining very promising simulation results, their physical system is behaving poorly. It is interesting that the authors do not give any comment about the working conditions of the rotors' engines. Even at the simulation stage, the controller they designed is requesting the rotors to operate in a bang-bang mode, even after obtaining correct attitude [32], p. 47. Taking additionally into account the specific linearization performed by the authors of [5] and [32], it is interesting to examine the same aspect in the extended model presented here. The control signals and motors' speeds in the test presented in section A of part IV of this article, after initial transients, are kept at a constant level, as presented in Fig. 13. During simulation appropriate constraints were imposed in the model to represent off-the-shelf components and their limitations in terms of maximal voltage or current, as well as rotational velocity. The inspection of actuators behaviour shows an obvious advantage of the design proposed in this article over the one in [5] and [32]. It follows from less demanding operation of the rotors and considerable savings in power required, as the biggest battery drain occurs during transients. However, to definitely state about the advantages of the design proposed in this article, the tests on physical object are necessary.

Models from [5, 12] and [13] in hover flight reduce to the same set of equations. It is though interesting to see what are the differences in the behaviour of model derived here when particular aspects of it are simplified to resemble the ones presented in [5, 12, 13] while still relying on LQ control. To analyse those differences the transition from hover to forward flight is scrutinized.

For that purpose the LQ regulator is constructed, each time using the same $Q$ and $R$ matrices, but the components of model are different. The results of those tests are presented in Fig. 14.

Figure 14 presents the angular rates of rotors during the transition from hover into forward flight for the extended model and the model equivalent to the one in [12], where gyroscopic effects are neglected. Appropriately designed LQ controller makes the differences in behaviour of quadrotor during transition from hover to forward flight negligible. In both models also the helicopter-characteristic behaviour of excess power climb [1, 23] is visible. Figure 14 (lower row) presents the behaviour of more simplified model during the same hover to forward flight transition. Here not only gyroscopic effects are neglected, but also the thrust is assumed constantly proportional to the square of rotor's angular velocity, as in [5–9, 32]. Not only quantitative, but also qualitative change is easy to notice comparing to Fig. 14, upper row. The rotors' rates are increased, when in reality they should be decreased to maintain a constant level of flight. Such behaviour may lead to a collision with any obstacle being above hovering craft, leading potentially to its crash. This emphasizes the importance of accurate description of aerodynamics and justifies the studies undertaken to develop more precise description of quadrotor platform dynamics.
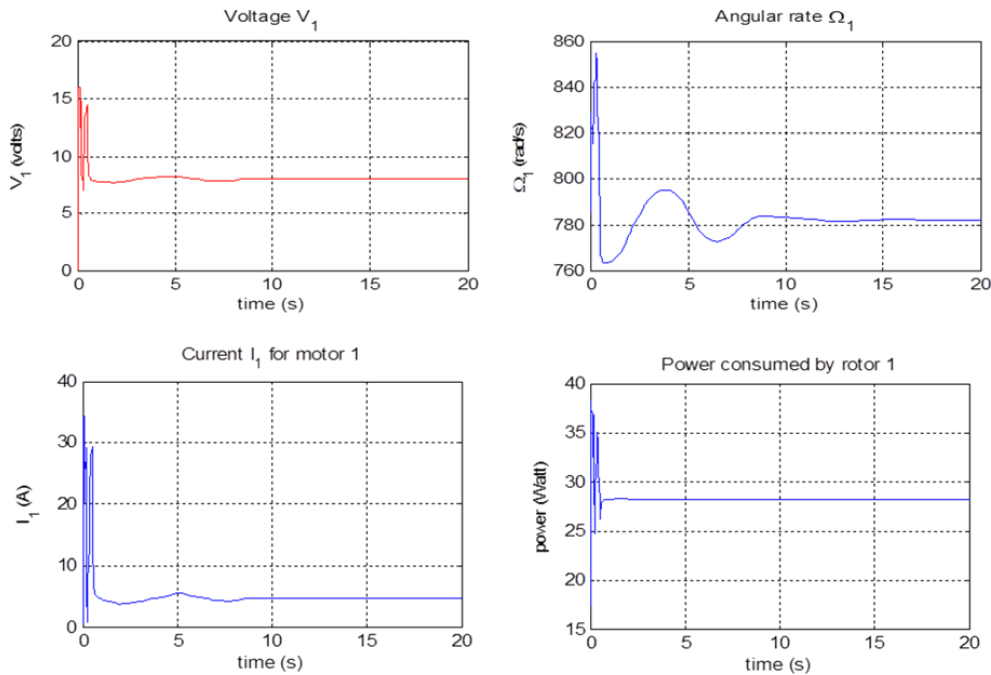


Fig. 13. Controller commanded voltage for motor 1 (left upper corner) and resulting motor rates, current and power consumed during attitude stabilization
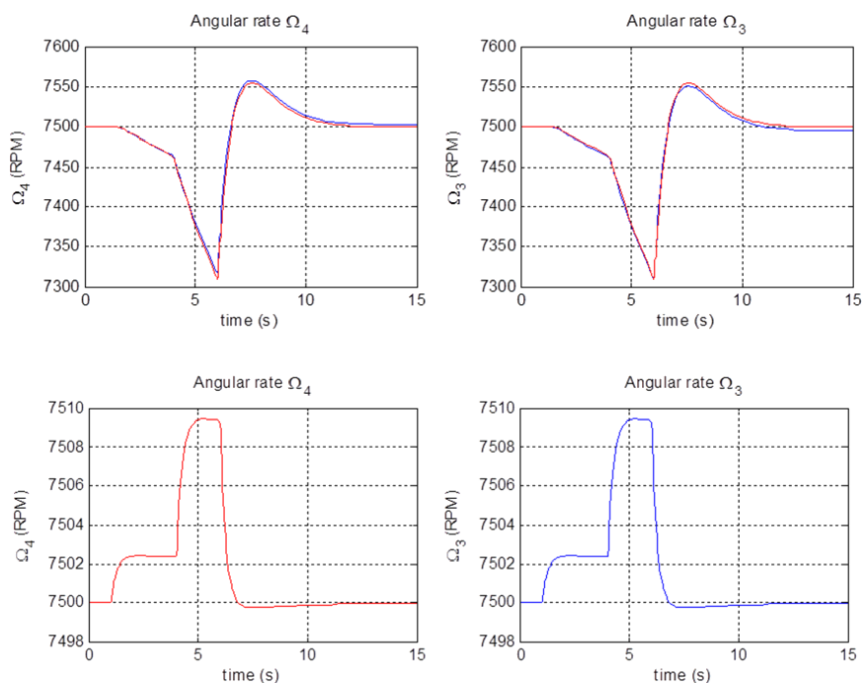
Fig. 14. Upper row: comparison of rotor angular rates for the extended dynamics model presented in this article (blue) and the model without gyroscopic effects (red) from Ref. [14]. Lower row: time responses of the angular rates of rotor for the model with simplified thrust description

**4.5. Influence of disturbances.** In this section a hovering capability, as well as following a predefined trajectory under wind gusts disturbances is examined. According to [33] the Statistical Discrete Gust (SDG) method is ideally suited for low-level helicopter applications, as it gives a possibility to asses a response to, and recovery from, large disturbances. Test results for disturbances, for the same hover flight and trajectory following as in sections A and C of part IV, are given in Figs. 15 and 16, respectively.
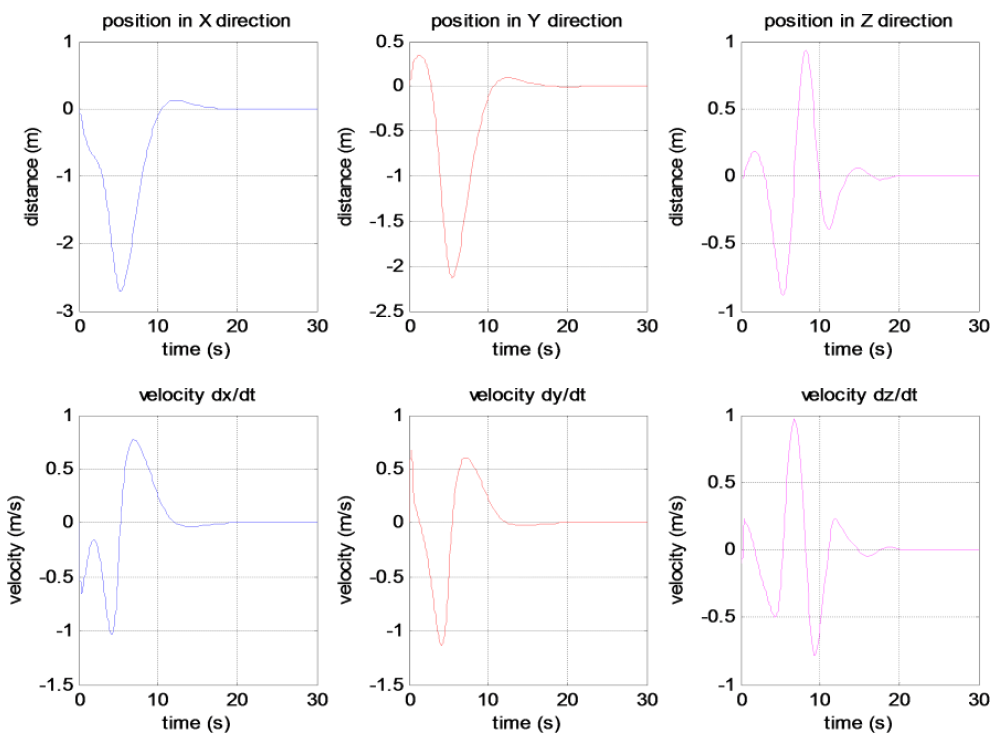


Fig. 15. Hover flight under SDG disturbance with amplitude 3.5 m in $X$ direction and 3 m in $Y$ direction, with rise time w.r.t. hovering quadrotor platform of 5 s

*Modelling and optimal control system design for quadrotor platform – an extended approach*
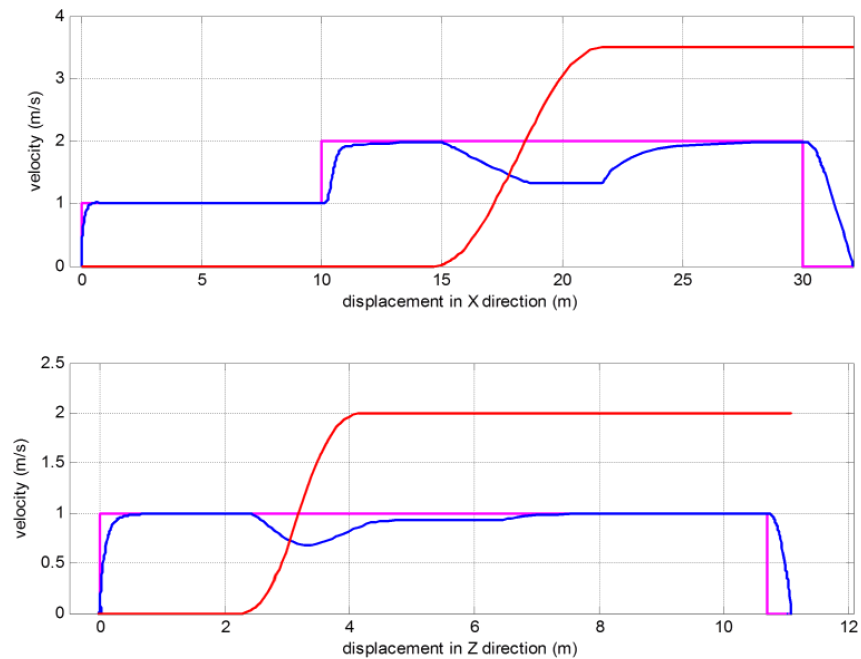


Fig. 16. Commanded velocity profile (magenta), system response (blue) and gust disturbance (red) for $X$ axis (upper picture) and $Z$ axis (lower picture). Gust is coming from a direction opposite to motion

The system shows to be fairly robust in terms of disturbance rejection. With total mass assumed of 1 kg it is able to maintain hover in designated spot in relatively harsh conditions. It is important to observe that although the simulated gust is strictly horizontal with no vertical component, the variation in platform's position and velocity along $Z$ axis of inertial system is considerable. It is caused by variation of thrust on each rotor due to variation in the inflow velocity. This scale of $Z$ axis motion is an inherent feature which cannot be compensated for by the change in regulator's settings. It originates in the fact that quadrotor with constant-pitch rotor blades is incapable of creating vertical downward thrust. Unless any aggressive manoeuvres are taken in account, it relays on gravity only for downward motion. This is a considerable drawback in constant-pitch quadrotor design, possibly limiting its applications and forcing caution when designing a flight trajectory or piloting the platform. Similar considerations are standing behind the recent development of variable-pitch quadrotors [34].

Following a predefined trajectory under disturbances is shown in Fig. 16. Under disturbances which magnitude is equal almost two times the set point value, a control system is able to maintain given flight parameters and even switch from forward flight to hover stop. Such robustness to external disturbances is partly resulting from embracing all state variables in the control loop. This is an easily obtainable feature in optimal control what constitutes another advantage of the approach proposed in this work and justifies research on enhanced model of quadrotor platform.

## 5. Conclusions

In this article an extended model of quadrotor platform was presented. In modelling of body dynamics the physical real-ization of the rotors' blades was taken into account, together with the associated gyroscopic effect. In modelling of aerodynamics the momentum theory was used to describe every phase of quadrotor's flight. The blade-flapping phenomenon was accounted for in the model. The controller choice was justified and the way of constructing the control system was described. Multiple simulation results were presented, showing that the system is capable of performing assigned tasks. These tests also showed which parts of the dynamic's model are important and which can be simplified without significant loss of model's accuracy. In that matter this article fills in the gap in discussion about possible intuitive simplifications of quadrotor model and the consequences they bring.

The results are very promising as they predict typical helicopter behaviour seldom present in preceding analysis of this subject, such as for e.g. excess power climb. This indicates high accuracy of the model. It also convinces the authors that it is possible to obtain a high precision and reliable full optimal control of quadrotor system. The entire community of researchers interested in this problem can benefit from solutions presented in this article, as in terms of tuning the behaviour of system under LQ control is intuitive and simple. At the cost of more advanced model, a relative simplification in terms of handling such flying platform is obtained.

In terms of future work, tests on the real system are the most important step. The description of platform built for that purpose can be found in [30, 35]. They will definitely reveal if here-designed model and LQ controller perform as expected. It is especially interesting to check whether an extended model presented here along with a dedicated controller will suffice for autonomous flight, which is a next logical step on the way of development of this project. It will also allow final conclusive comparisons with previous work in this field.

REFERENCES

[1] J. Leishman, *Principles of Helicopter Aerodynamics*, $2^{nd}$ ed., Cambridge University Press, New York, 2006.

[2] S. Anderson, "Historical overview of V/STOL aircraft technology", in *NASA Technical Memorandum 81280*, Ames Research Center, Moffett Field, 1981.

[3] N. Metni, J-M. Pflimlin, T. Hamel, and P. Soueres, "Attitude and gyro bias estimation for a VTOL UAV", *Control Eng. Pract.* 14, 1511–1520 (2006).

[4] A. Babiarz, R. Bieda, K. Jaskot, and J. Klamka, "The dynamics of the human arm with an observer for the capture of body motion parameters", *Bull. Pol. Ac.: Tech.* 61 (4), 955–971 (2013).

[5] S. Bouabdallah, A. Noth, and R. Siegwart, "PID vs. LQ control techniques applied to an indoor micro quadrotor", *2004 IEEE/RSJ Int. Conf. on Intelligent Robots and Systems* 3, 2451-2456 (2004).

[6] S. Bouabdallah, P. Murrieri, and R. Siegwart, "Design and control of an indoor micro quadrotor", *ICRA '04 IEEE Int. Conf. on Robotics and Automation* 5, 4393–4398 (2004).

[7] P. Corke, R. Mahony, and P. Pounds, "Modelling and control of a quad-rotor robot", *Proc. Australasian Conf. on Robotics and Automation* 1, CD-ROM (2006).

[8] T. Hamel, R. Lozano, R. Mahony, and J. Ostrowski, "Dynamic modelling and configuration stabilization for an X4-flyer", *15th Triennial World Congress Int. Federation of Automatic Control* 1, 846–848 (2002).

[9] P. Hynes, R. Mahony, P. Pounds, and J. Roberts, "Design of a four rotor aerial robot", *Australasian Conf. on Robotics and Automation* 1, 145–150 (2002).

[10] Penn State GRASP Laboratory https://www.grasp.upenn.edu/success_stories (2012).

[11] ETH Flying Machine Arena http://www.idsc.ethz.ch/Research_DAndrea/FMA (2012).

[12] G. Hoffman, H. Huang, C. Tomlin, and S. Waslander, "Quadrotor helicopter flight dynamics and control: theory and experiment", *AIAA Guidance, Navigation and Control Conf. and Exhibit* 1, CD-ROM (2007).

[13] P. Corke, J. Gresham, R. Mahony, P. Pounds, and J. Roberts, "Towards dynamically-favourable quad-rotor aerial robots", *2004 Australasian Conf. on Robotics & Automation* 1, CD-ROM (2004).

[14] P. Corke, R. Mahony, and P. Pounds, "Modelling and control of a large quadrotor robot", *Control Eng. Pract.* 18 (7), 691–699 (2010).

[15] P. Corke, R. Mahony, and P. Pounds, "Modelling and control of a large quadrotor robot", http://eprints.qut.edu.au/33732/1/cep2009_modelling_and_control_paper_sub_final.pdf (2012).

[16] G. Hoffman, C. Tomlin, and S. Waslander, "Quadrotor helicopter trajectory tracking control", *AIAA Guidance, Navigation and Control Conf. and Exhibit* 1, CD-ROM (2008).

[17] H. Bouadi, M. Bouchoucha, and M. Tadjine, "Sliding mode control based on backstepping approach for an UAV type-quadrotor", *Int. J. App. Math.* 4 (1), 12–17 (2007).

[18] R. Czyba, "Design of attitude control system for an UAV type-quadrotor based on dynamic contraction method", *IEEE/ASME Int. Conf. on Advanced Intelligent Mechatronics* 1, 644–649 (2009).

[19] A. Mokhtari, A. Benallegue, and B. Daachi, "Robust Feedback Linearization and $H_{\infty}$ controller for a quadrotor unmanned aerial vechicle", *J. Electr. Eng.* 57 (1), 20–27 (2006).

[20] R. Zawiski and M. Błachuta, "Dynamics and optimal control of quadrotor platform", *AIAA Guidance, Navigation and Control Conf. and Exhibit* 1, CD-ROM (2012).

[21] R. Zawiski, "Control-oriented modelling of quadrotor UAV platform", *Ph.D. Dissertation*, Institute of Automatics, Faculty of Automatics, Electronics and Computer Science, Silesian University of Technology, Gliwice, 2012.

[22] R. Prouty, *Helicopter Performance, Stability and Control*, Krieger Publishing Company, Malabar, 2002.

[23] A. Bramwell, G. Done, and D. Blamford, *Bramwell's Helicopter Dynamics*, $2^{nd}$ ed., Butterworth-Heinemann, Woburn, 2001.

[24] S. Baldursson, "BLDC motor modelling and control-a MATLAB/SIMULINK implementation", *Master Thesis*, Chalmers University of Technology, Gothenburg, http://web-files.portal.chalmers.se/et/MSc/BaldurssonStefanMSc.pdf (as of 06.2012), 2005.

[25] M. Drela, "First-order DC electric motor model", *MIT Aero and Astro*, 2007, http://web.mit.edu/drela/Public/web/qprop/motor1_theory.pdf (2012).

[26] B. Szlachetko and M. Lower "Stabilisation and steering of quadrocopters using fuzzy logic regulators", $11^{th}$ *Int. Conf. on Artificial Intelligence and Soft Computing* PT 1, 691–698 (2012).

[27] A. Dzieliński and P.M. Czyronis, "Fixed final time and free final state optimal control problem for fractional dynamic systems – linear quadratic discrete-time case", *Bull. Pol. Ac.: Tech.* 61 (3), 681–690 (2013).

[28] R. Zawiski and M. Błachuta, "Model development and optimal control of quadrotor aerial robot", *IEEE $17^{th}$ Int. Conf. on Methods and Models in Automation and Robotics* 1, 475–480 (2012).

[29] R. Zawiski and M. Błachuta, "Chosen aspects of modelling and control of quadrotor platform", $9^{th}$ *Int. Conf. on Mathematical Problems in Engineering, Aerospace and Sciences* 1, 1116-1123 (2012).

[30] R. Czyba and G. Szafrański "Control structure impact on the flying performance of the multi-rotor VTOL platform – design, analysis and experimental validation", *Int. J. Adv. Robot. Syst.* 10 (62), 1–9 (2013).

[31] M.G. Ballin, *Validation of Real-Time Engineering Simulation of the UH-60 Helicopter*, NASA Technical Memorandum 88360, 1987.

[32] A. Noth, "*Synthèse et implémentation d'un contrôleur pour micro hélicoptère à 4 rotors*", *Diploma Project*, Swiss Federal Institute of Technology, Lausanne, 2004.

[33] G. Padfield, *Helicopter Flight Dynamics: the Theory and Application of Flying Qualities and Simulation Modelling*, $2^{nd}$ ed., Blackwell Publishing, Oxford, 2007.

[34] M. Cutler, J. How, B. Michini, and N. Ure, "Comparison of fixed and variable pitch actuators for agile quadrotors", *AIAA Guidance, Navigation, and Control Conf. and Exhibit* 1, CD-ROM (2011).

[35] G. Szafrański, R. Czyba, W. Janusz, and W. Błotnicki, "Altitude estimation for the UAV's applications based on sensors fusion algorithm", *Int. Conf. on Unmanned Aircraft Systems* 1, 508–515 (2013).